

# Transverse Energy per Charged Particle in Heavy-Ion Collisions: Role of Collective Flow

Swatantra Kumar Tiwari and Raghunath Sahoo\*

*Discipline of Physics, School of Basic Sciences, Indian Institute of Technology Indore, Indore- 453552, INDIA*

(Dated: February 3, 2017)

The ratio of (pseudo)rapidity density of transverse energy and the (pseudo)rapidity density of charged particles, which is a measure of the mean transverse energy per particle, is an important observable in high energy heavy-ion collisions, which reveals about the mechanism of particle production and the freeze-out criteria. Its collision energy and centrality dependence is exactly like the chemical freeze-out temperature till top RHIC energy. The LHC measurement at  $\sqrt{s_{NN}} = 2.76$  TeV brings up new challenges to rule out the mechanisms of gluon saturation or non-equilibrium phenomena being prevalent at high energies, which could contribute to the above observable. The Statistical Hadron Gas Model (SHGM) with a static fireball approximation has been successful in describing both the centrality and energy dependence till top RHIC energies. However, the SHGM predictions for higher energies are highly underestimated by the LHC data. In order to understand this, we have incorporated radial flow effect in an excluded volume SHGM. The hard-core radius of baryons at lower collision energies plays an important role in the description of a hadronic system. In view of this, in order to make a complete energy dependence study from FAIR to LHC energies, we have considered an excluded volume SHGM. Our studies suggest that the collective flow plays an important role in describing  $E_T/N_{ch}$  and it could be one of the possible parameters to explain the jump observed in  $E_T/N_{ch}$  from RHIC to LHC energies. Predictions for the LHC measurements at  $\sqrt{s_{NN}} = 5.02$  TeV are given.

PACS numbers: 12.38.Mh, 25.75.Nq, 24.10.Pa

## I. INTRODUCTION

The transverse energy and charged particle multiplicity at midrapidity are one of the first measurements done in heavy-ion collision experiments at (ultra)relativistic energies, as global observables to characterize the system formed in these collisions. These two are very important observables, as they are directly associated with the collision geometry and collision energy. Heavy-ion collisions at AGS, SPS, RHIC and LHC energies aim to produce a partonic phase of matter and study the Quantum Chromodynamics (QCD) deconfinement transition and explore/scan the QCD phase diagram for a possible location of the critical point (CP), by controlling the temperature and baryochemical potential by changing the collision species/centrality and collision energy. In these efforts the future facilities like CBM experiment at FAIR energies ( $E_{lab}$  : 10 AGeV-40 AGeV) and the LHC and beyond (FCC, ILC) would play a pivotal role in exploring the QCD phase boundary, and establishing the nature of the QCD phase transition and the location of CP. The discovery of a strongly interacting partonic matter at RHIC, which behaves like a liquid with lowest  $\eta/s$  ratio [1–4], and is comparable with the ADS/CFT calculations [5], small systems (p+p collisions) at LHC showing collectivity [6], which is a possible signature of Quark-Gluon Plasma (QGP) (initially expected to be formed only in top central heavy-ion collisions) and the energy

loss patterns of heavy-quarks in the medium formed at the LHC are few very important aspects of the new states of matter formed at ultra-relativistic energies. The matter formed at LHC energies has seen to show properties very different from that is observed at RHIC in many aspects, *i.e.* suppression of  $J/\psi$  [7] and other quarkonia,  $\frac{dE_T}{d\eta(y)} / \frac{dN_{ch}}{d\eta(y)} \equiv E_T/N_{ch}$  showing behaviour not expected by equilibrium Statistical Hadron Gas Model (SHGM) with a static fireball approximation [8–10], the collision energy dependence of  $dN_{ch}/d\eta$  deviating from a logarithmic behaviour etc. There is a need to study the global observables like  $E_T/N_{ch}$  in more details including the collectivity in the system to rule out any possible effect of non-equilibrium phenomena or the effect of gluon saturation, which is expected at higher collision energies, to play a role at LHC energies.

The pseudo(rapidity) density of transverse energy,  $dE_T/d\eta(y)$  is an approximate Lorentz invariant measure of the energy distribution and is a measure of the explosiveness of the collision. This is an important observable, as it is the energy of the produced particles in the transverse phase space, which was completely empty before the collision. The energy of the incoming nuclei in the longitudinal direction is converted to the energy of the produced secondaries. The midrapidity measurement of  $dE_T/dy$  is related to the initial energy density of the system. In longitudinal boost invariant Bjorken hydrodynamics, this helps in making a direct comparison with the lattice QCD prediction of energy density for a deconfinement transition and thereby giving a first hint of a possible partonic medium. The study of the centrality and collision energy dependence of  $dE_T/dy(\eta)$  sheds light

---

\*Corresponding author: *Raghunath.Sahoo@cern.ch*

on possible freeze-out criteria in heavy-ion collisions [8].

Recently using an excluded-volume statistical hadron gas model (EV-SHGM) with the longitudinal flow, we have studied the limiting fragmentation (LF) phenomenon in the rapidity spectra of  $\pi^+$  in heavy-ion collisions. Here, we found that the LF is violated at top RHIC and LHC energies [11], which goes inline with the expectations for higher energies, where the inelastic cross-section is shown to increase with collision energy. In this paper, we study the variation of  $E_T/N_{ch}$  with respect to centrality and centre-of-mass energy ( $\sqrt{s_{NN}}$ ) over a broad energy range from 2.7 GeV to 5.02 TeV using EV-SHGM with radial flow. Experimentally,  $E_T/N_{ch}$  increases at lower energies rapidly and then it saturates around SPS energies upto top RHIC energy. Till lower SPS energies, the increase in collision energy increases the mean energy or transverse mass ( $m_T$ ) of each particle. From SPS to RHIC energies, the additional energy pumped into the system in terms of the increase in  $\sqrt{s_{NN}}$ , goes for new particle production [8, 9]. Recently, the experimental data at LHC energy of 2.76 TeV show a jump in this spectrum due to furthermore increase in mean energy or  $m_T$  [9], and possible collective effects which does not follow a static fireball expectations. In order to understand this at LHC energies, we use our recently proposed model, where we incorporate the attractive interactions by including the resonances upto the mass of 2 GeV and repulsive interactions by assigning the geometrical hard-core size to each baryon. Mesons are treated as pointlike particles in our model. We also incorporate the collective flow in our model to explain the experimental data at various energies particularly at LHC energies. In ref. [12], the statistical model is also used to study the transverse energy per charged particle at midrapidity with longitudinal and transverse flows for the wide range of energies from AGS to RHIC. In our case, we do not take volume as a free parameter and extend our analysis upto LHC energies, where the role of collective flow is more pronounced than at lower energies. In addition, we study the centrality dependence

of  $E_T/N_{ch}$  at top RHIC and LHC energies, which is related to the chemical freeze-out of the system. We study the energy dependence of the associated observables like the participant pair normalized- $\frac{dE_T}{dy(\eta)}$ , the Bjorken energy density ( $\epsilon_{Bj}$ ) in order to study the created system at different energies and the possible different behaviour at LHC energies, which could serve the purpose of ruling out and/or establishing different production mechanisms. In our model calculation, we assume that the chemical and thermal freeze-outs occur simultaneously which infers the absence of the possible elastic scattering after chemical freeze-out [13, 14].

The paper is organized as follows: in section-II, we give the formulation of the SHGM with an excluded volume correction and the method of inclusion of collective flow. In section-III, we show the results and in section-IV, we discuss the relation of  $E_T/N_{ch}$  with various freeze-out criteria. In section V, we give the summary with outlook and open problems.

## II. FORMULATION OF THE MODEL

The formula for the number density of the i-th baryon in the Maxwell-Boltzmann's statistics can be written as [15] :

$$n_i^{ex} = (1 - R)I_i\lambda_i - I_i\lambda_i^2 \frac{\partial R}{\partial \lambda_i}, \quad (1)$$

where  $R = \sum_i n_i^{ex} V_i^0$  is the fractional occupied volume

by the baryons [16].  $V_i^0 = (4\pi r'^3)/3$  is the eigen-volume of each baryon having a hard-core radius  $r'$  and  $\lambda_i$  is the fugacity of the i-th baryon. Here we take  $r' = 0.8 fm$ , which is the only free parameter in the discussed model.  $I_i$  is the momentum integral for baryons in the Boltzmann's statistics. Eq. (1) can be reduced in the following form [17, 18] :

$$\frac{dN_i}{dy m_T dm_T d\phi} = \frac{g_i V \lambda_i}{(2\pi)^3} \left[ \left( (1 - R) - \lambda_i \frac{\partial R}{\partial \lambda_i} \right) \frac{E_i}{\left[ \exp \left( \frac{E_i}{T} \right) \right]} \right]. \quad (2)$$

---

Here  $y$  is the rapidity variable and  $m_T = \sqrt{m^2 + p_T^2}$  is the transverse mass.  $E_i$  is the energy of the i-th baryon,  $V$  is the total volume of the fireball formed at chemical freeze-out and  $N_i$  is the total number of the i-th baryon.

---

We assume that the volume of the fireball,  $V$  is the same for all types of hadrons at the time of the homogeneous emissions.

By using  $E_i = m_T \cosh y$ , eq. (2) can be written as [18]:

$$\frac{dN_i}{dy m_T dm_T d\phi} = \frac{g_i V \lambda_i}{(2\pi)^3} \left[ \left( (1-R) - \lambda_i \frac{\partial R}{\partial \lambda_i} \right) \frac{m_T \cosh y}{\left[ \exp \left( \frac{m_T \cosh y}{T} \right) \right]} \right]. \quad (3)$$

### A. Transverse Energy of Hadrons in a Thermal Model

The transverse energy,  $E_T$  in an event is defined as:

$$E_T = \sum_i E_i \sin \theta_i, \quad (4)$$

with  $\theta_i$  as the polar angle made by the i-th particle in an event with the detector. The sum is taken over all the particles emitted into a fixed solid angle within the detector acceptance. Taking into account the calorime-

try measurement of  $E_T$ , one redefines the energy of the individual secondaries as [19–21]

$$E_i = \begin{cases} E_{\text{total}} - m & \text{for baryons} \\ E_{\text{total}} + m & \text{for anti-baryons} \\ E_{\text{total}} & \text{for all other particles.} \end{cases} \quad (5)$$

Considering the above experimental formulae, we proceed with the formulation of the transverse energy in our excluded-volume model. Using eq. (3), we write the energy of the i-th baryon per unit rapidity as :

$$\frac{dE_i}{dy} = \frac{g_i V \lambda_i}{(2\pi^2)} \left[ \left( (1-R) - \lambda_i \frac{\partial R}{\partial \lambda_i} \right) \right] \int \frac{m_T^3 \cosh^2 y dm_T}{\left[ \exp \left( \frac{m_T \cosh y}{T} \right) \right]}. \quad (6)$$

Similarly, the energy of the m-th meson per unit rapidity can be calculated as :

$$\frac{dE_m}{dy} = \frac{g_m V \lambda_m}{(2\pi^2)} \int \frac{m_T^3 \cosh^2 y dm_T}{\left[ \exp \left( \frac{m_T \cosh y}{T} \right) \right]}. \quad (7)$$

Here,  $g_m$  and  $\lambda_m$  are the degeneracy factor and fugacity of the m-th meson. The above equations give the

transverse energy of the particles in a stationary thermal source.

### B. Transverse Energy of Hadrons in a Thermal Model with Flow

The invariant yield with the inclusions of collective flow can be written as [22] :

$$\frac{dN_i}{m_T dm_T dy d\phi} = \frac{g_i V \lambda_i m_T}{(2\pi)^3} \left[ (1-R) - \lambda_i \frac{\partial R}{\partial \lambda_i} \right] \int \exp \left( - \frac{m_T \cosh(y-\eta) \cosh \rho - p_T \sinh \rho \cos \phi}{T} \right) r dr d\zeta. \quad (8)$$

Here,  $\rho$  is the parameter given by  $\rho = \tanh^{-1} \beta_r$ , with the profile chosen as  $\beta_r = \beta_s \left( \xi \right)^n$  [22, 23].  $\beta_s$ , the maximum surface velocity appears as a free parameter in our model calculation and  $\xi = \left( r/R_0 \right)$ ,  $R_0$  is the maximum radial position of the fireball at freeze-out. The average of the radial flow can be calculated by the following formula [24] :

$$\langle \beta_r \rangle = \frac{\int \beta_s \xi^n \xi d\xi}{\int \xi d\xi} = \left( \frac{2}{2+n} \right) \beta_s. \quad (9)$$

For the sake of simplicity, we take  $n=1$  in our model calculation. After incorporating the collective flow in our thermal model, we get the expressions for energy of baryons per unit rapidity as follows :

$$\frac{dE_i}{dy} = \frac{g_i V \lambda_i}{(2\pi)^3} \left[ (1 - R) - \lambda_i \frac{\partial R}{\partial \lambda_i} \right] \int \exp \left( - \frac{m_T \cosh(y - \eta) \cosh \rho - p_T \sinh \rho \cos \phi}{T} \right) m_T^3 \cosh^2 y r dr d\phi d\zeta dm_T, \quad (10)$$

where  $r$  lies between 0 and  $R_0$  i.e. the radius of the fireball at freeze-out, the azimuthal angle  $\phi$  lies between 0 and  $2\pi$ , and the longitudinal space-time rapidity variable

$\zeta$  varies between  $-\eta_{max}$  and  $\eta_{max}$ . In a similar fashion, we can calculate the energy of the  $m$ -th meson by using the following formula :

$$\frac{dE_m}{dy} = \frac{g_m V \lambda_m}{(2\pi)^3} \int \exp \left( - \frac{m_T \cosh(y - \eta) \cosh \rho - p_T \sinh \rho \cos \phi}{T} \right) m_T^3 \cosh^2 y r dr d\phi d\zeta dm_T. \quad (11)$$

Here,  $E_m$ ,  $g_m$ , and  $\lambda_m$  represent the energy, degeneracy factor and fugacity of the  $m$ -th meson. Now, eq. (4) can be reduced in the following form :

$$\langle E_T \rangle = \left\langle \sum_i E_i \sin \theta_i \right\rangle. \quad (12)$$

The average of  $\sin \theta$  can be calculated as follows :

$$\langle \sin \theta \rangle = \frac{1}{4\pi} \int \sin \theta d\Omega = \frac{1}{4\pi} \int \sin^2 \theta d\theta d\phi,$$

where  $d\Omega (= \sin \theta d\theta d\phi)$  is the solid angle. Now, integrating above equation we get :

$$\langle \sin \theta \rangle = \frac{1}{4\pi} \int_0^\pi \sin^2 \theta d\theta \int_0^{2\pi} d\phi = \frac{\pi}{4}.$$

Now, we can write the expression of the transverse energy of hadrons as follows [8] :

$$\langle E_T \rangle = \frac{\pi}{4} \left[ \langle E \rangle - m_N \langle N_B - N_{\bar{B}} \rangle \right]. \quad (13)$$

$\langle E \rangle$  is the total energy of hadrons.  $N_B - N_{\bar{B}}$  is the net-baryon which can be calculated by using eq. (1). After obtaining the transverse energy, we calculate the Bjorken energy density by using the following formula:

$$\epsilon_{Bj} = \frac{dE_T}{dy} \frac{1}{\tau \pi R^2}, \quad (14)$$

where  $\tau$  is the formation time and  $\pi R^2$  is the transverse overlap area of the colliding nuclei. There are various ways to quantify the overlap area. Here,  $R$  is the radius of the colliding nuclei given by  $R = R_0 A^{1/3}$ . Replacing  $A$  by  $N_{part}/2$ , where  $N_{part}$  is the number of nucleon participants [25],  $\epsilon_{Bj}$  becomes

$$\epsilon_{Bj} = \frac{dE_T}{dy} \frac{1}{\tau \pi R_0^2 \left( N_{part}/2 \right)^{2/3}}. \quad (15)$$

### III. RESULTS AND DISCUSSIONS

In order to calculate the ratio  $E_T/N_{ch}$ , we estimate  $N_{ch}$  in our model in terms of the number of primarily produced particles,  $N$ . We follow the same procedure as done in ref. [8]. We first estimate the ratio of the total number of hadrons in final state,  $N_{decays}$  to the total number of primordial hadrons,  $N$  with respect to  $\sqrt{s_{NN}}$  over a broad energy range from AGS to LHC energies using EV-SHGM as shown in the upper panel of figure 1. Now, we study the ratio of the number of charged hadrons,  $N_{ch}$  to  $N_{decays}$  with  $\sqrt{s_{NN}}$  from AGS to LHC energies as shown in the lower panel of the figure 1. In order to calculate these ratios, we use the chemical freeze-out temperature ( $T$ ), and baryon chemical potential ( $\mu_B$ ) at each  $\sqrt{s_{NN}}$  as mentioned in ref. [26]. We find that the ratio  $N_{decays}/N$  initially increases rapidly with  $\sqrt{s_{NN}}$ , because the production of resonances increases with energy and become saturated at SPS energies around a value of 1.7, where chemical freeze-out temperature becomes independent of collision energy. Similarly, the ratio  $N_{ch}/N_{decays}$  also increase with  $\sqrt{s_{NN}}$  and gets saturated at SPS energies around 0.6. Although, these findings are the same as observed in [8] but the difference occurs at lower energies where the excluded-volume correction is more effective.

In this paper, we want to study the variations of  $E_T/N_{ch}$  with respect to centrality for various  $\sqrt{s_{NN}}$ . For this purpose, we connect centrality in terms of number of participants ( $N_{part}$ ) with  $T$  and  $\mu_B$  by studying the centrality dependence of particle ratios in our model. Figure 2 represents the variations of various hadron ratios such as  $K^+/\pi^+$ ,  $K^-/\pi^-$ ,  $K^-/K^+$ , and  $\bar{p}/p$  with respect to number of participants,  $N_{part}$  for Au-Au collisions at  $\sqrt{s_{NN}} = 200$  GeV. In order to calculate  $N_{part}$  dependence of ratios, we relate the freeze-out parameters  $T$  and  $\mu_B$  with  $N_{part}$  at this energy. We select three centrality bins with participant numbers  $328 \pm 6$  (most-central),  $140 \pm 11$  (mid-central), and  $62 \pm 10$  (peripheral) while calculating the particle ratios. We find that the freeze-out

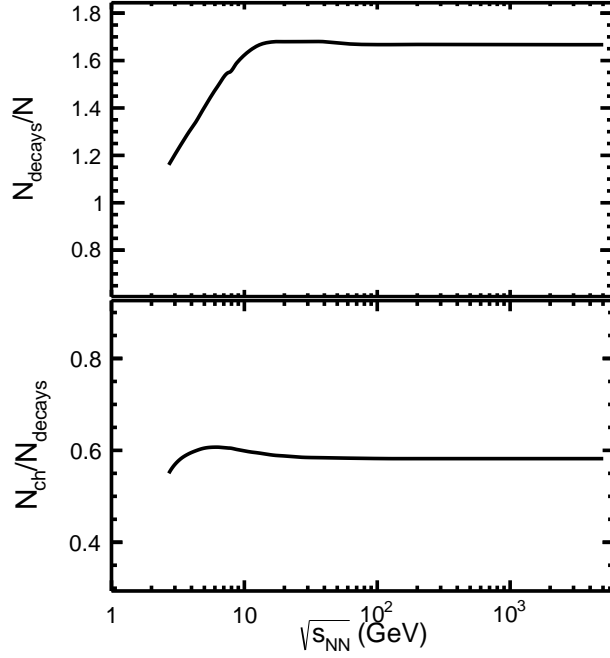


FIG. 1: The variation of  $N_{decays}/N$  (upper panel) and  $N_{ch}/N_{decays}$  (lower panel) with  $\sqrt{s_{NN}}$  at chemical freeze-out.

parameters  $T$  and  $\mu_B$  do not vary much with  $N_{part}$ . Having done these, we compare our model predictions with the experimental data [27]. We find that our model explains the data very well over all the centralities. For the sake of convenience, we take the strangeness saturation factor ( $\gamma_s$ ) equals 1 over all the centrality at this energy. In ref. [28], the detailed analysis of variations of particle ratios with centrality is done using the variation of  $\gamma_s$  with  $N_{part}$ .

In figure 3, we show the variations of  $E_T/N_{ch}$  with  $N_{part}$  for Au-Au collisions at  $\sqrt{s_{NN}} = 200$  GeV. We take the same value of  $T$  and  $\mu_B$  as used in the calculation of the hadron ratios with respect to  $N_{part}$  at this energy while studying the  $N_{part}$  dependence of  $E_T/N_{ch}$ . We also compare our results with the experimental data [19] and find a very good agreement between these two. In our calculation, we take the same centrality bins as used in the calculation of particle ratios at this energy.  $E_T/N_{ch}$  is almost independent of centrality except at lower centrality bins with the participant number less than 100. The present model explains the data well except at a lower  $N_{part}$ . We also show the obtained results with collective flow which explains the data within the experimental errors.

Figure 4 represents the centrality dependence of various hadrons ratios for Pb-Pb collisions at  $\sqrt{s_{NN}} = 2.76$  TeV. To calculate the particle ratios with respect to  $N_{part}$ , we relate  $T$  and  $\mu_B$  with  $N_{part}$  at this energy. Once we get the variations of freeze-out parameters with  $N_{part}$ , we calculate various particle ratios. While calculating ratios with respect to  $N_{part}$ , we select three

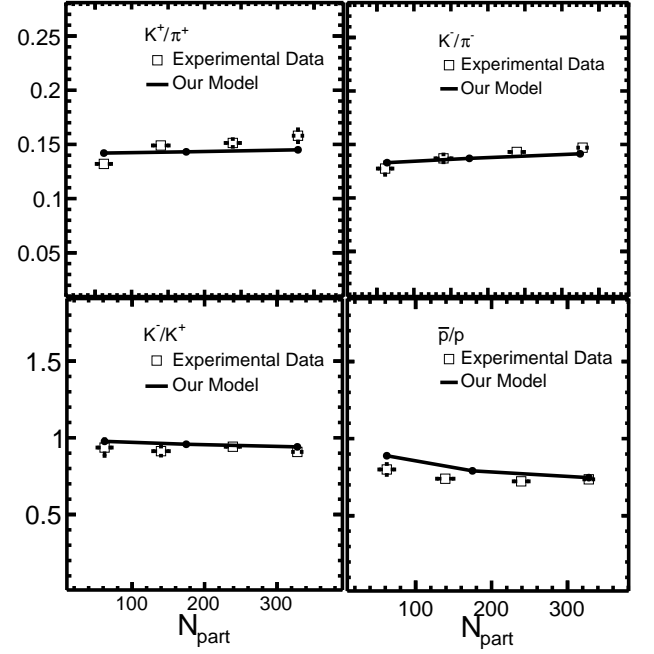


FIG. 2: The variations of particle ratios for Au-Au collisions with respect to number of participants at  $\sqrt{s_{NN}} = 200$  GeV. Symbols show the experimental data [27] and lines are our model calculations.

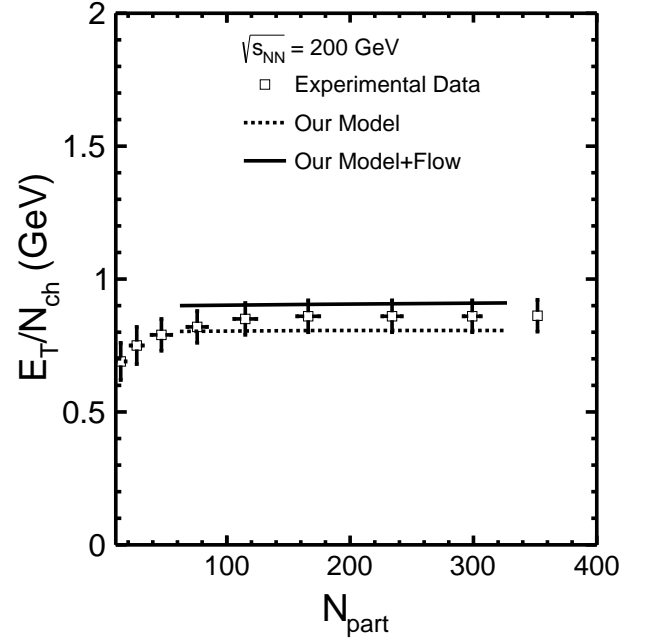


FIG. 3: Transverse energy per charged particle vs number of participants for Au-Au collisions at  $\sqrt{s_{NN}} = 200$  GeV. Symbols are the experimental data [19]. Solid line is the result obtained in our model with flow while dotted line is the result of our model calculations.

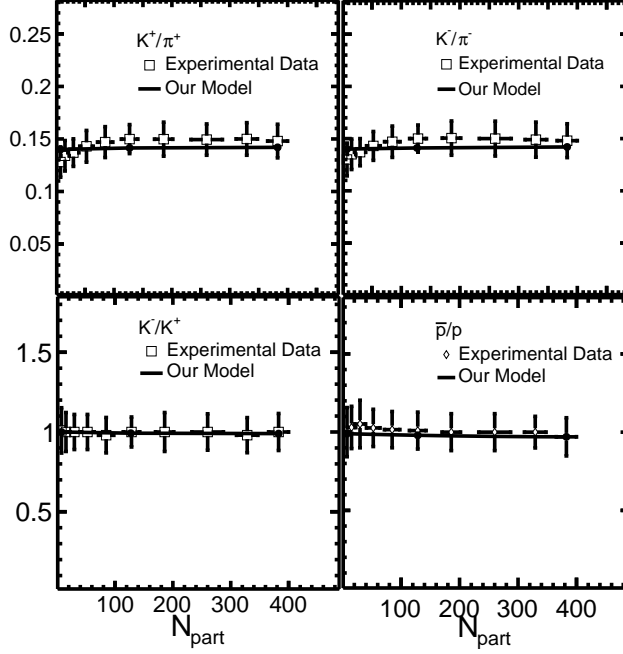


FIG. 4: The variations of hadron ratios for Pb-Pb collisions with respect to  $N_{part}$  at  $\sqrt{s_{NN}} = 2.76$  TeV. Symbols show the experimental data [29] and lines are our model results.

centrality bins in our model with participant numbers  $382 \pm 17$  (most-central),  $128 \pm 16$  (mid-central), and  $7 \pm 4$  (peripheral). Again, we take  $\gamma_s$  equal to one over all the centrality for the sake of simplicity. We compare our results with the experimental data [29] and again, find that our model explains the data very well over all the centralities.

Now, we need to know  $\sqrt{s_{NN}}$  dependence of chemical freeze-out volume in unit slice of rapidity to calculate transverse momentum spectra, transverse energy at midrapidity etc. Figure 5 describes the chemical freeze-out volume ( $dV/dy$ ) for  $\pi^-$  for the most central collisions at various  $\sqrt{s_{NN}}$  starting from 2.7 GeV to 5.02 TeV calculated in our model with Boltzmann approximation. To calculate the  $dV/dy$  for  $\pi^-$ , we use the experimental midrapidity yield of  $\pi^-$  [30] and divide it by the corresponding number density calculated in our model. At  $\sqrt{s_{NN}}=5.02$  TeV, we use the AMPT data for the midrapidity yield for  $\pi^+$  [31] in the absence of the experimental data. We compare our model results with the HBT data [32, 33], which represents the kinetic freeze-out volume, and find that our model results follow the same trend as observed in the HBT data. While HBT data correspond to the kinetic freeze-out volume, our calculations refer to the volume of the fireball at chemical freeze-out. A lower value from our estimation is thus expected. Figure 6 demonstrates the transverse mass spectra of positive pions for the most central collisions at  $\sqrt{s_{NN}} = 2.7$  GeV. We compare our calculations with flow, represented by the solid line, with the experimental data [34]. We notice a good agreement between experimental data and

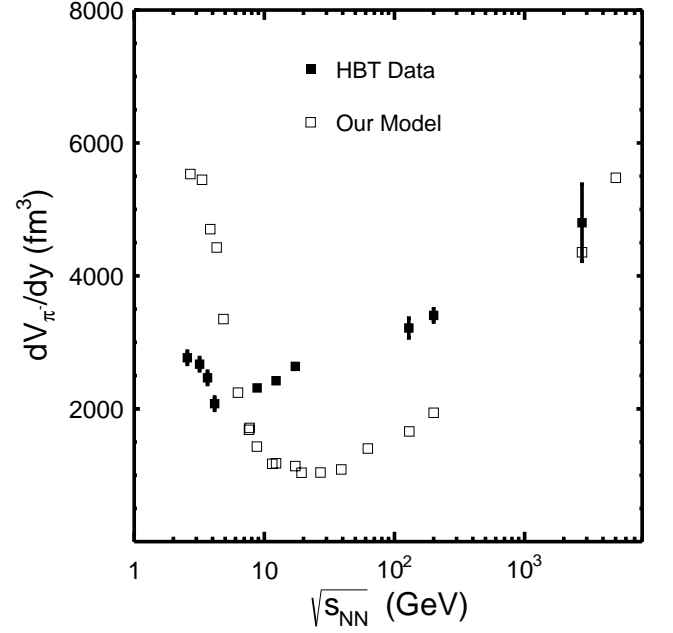


FIG. 5: The variations of freeze-out volume for  $\pi^-$ . Solid symbols are HBT data points [32, 33] and open symbols are those obtained in our model calculations.

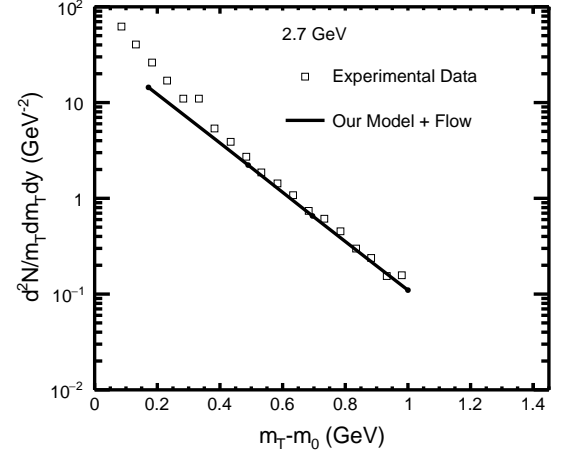


FIG. 6: The transverse mass spectra of  $\pi^+$  at  $\sqrt{s_{NN}} = 2.7$  GeV. Symbols are experimental data [34] while line is our result.

model calculations. After comparison, we get the value of the surface velocity,  $\beta_s$  which gives the value of the radial flow at this energy.

In figure 7, we show the  $p_T$  spectra of  $\pi^-$  for the most central collisions at various  $\sqrt{s_{NN}}$  from 7.7 GeV to 62.4 GeV. We use our model with the effect of flow to calculate  $p_T$ -spectra at all energies where we take only the surface velocity,  $\beta_s$  as a free parameter. We compare our results with the experimental data [35–38] and find that our model with flow explains the data satisfactorily. Af-



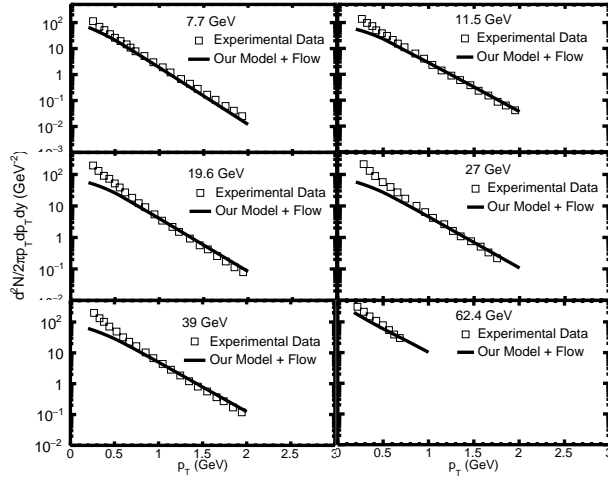


FIG. 7: The transverse momentum spectra of  $\pi^-$  at various energies. Symbols are experimental data while lines are our model results with flow.

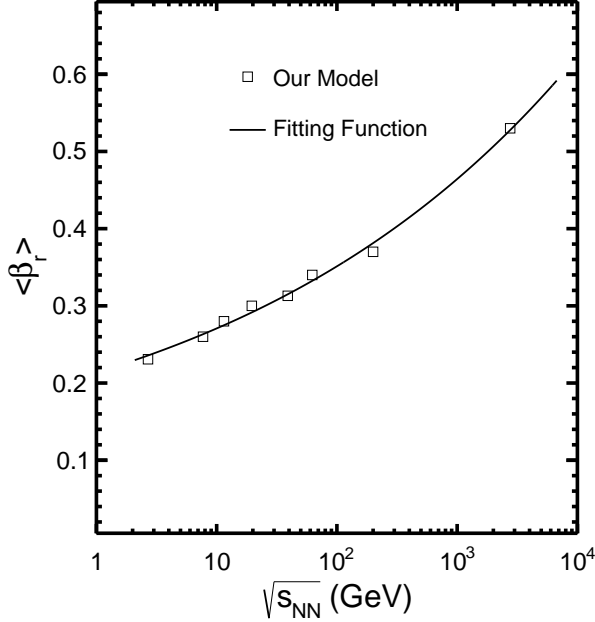


FIG. 8: The variations of the radial flow velocity ( $\langle\beta_r\rangle$ ) extracted in our model with respect to  $\sqrt{s_{NN}}$ . The solid line is a power-law fit as mentioned in the text.

ter comparison with the experimental data, we get the value of the  $\beta_s$ , from which we calculate the average radial flow velocity. Here, our model with flow explains the experimental data successfully except at lower  $p_T$ , where the contribution of resonance decay plays an important role [30]. In this paper, we do not take the contributions of resonance decays while calculating  $p_T$  spectra and we reserve this for a future work.

Figure 8 shows the variations of average radial flow velocity,  $\langle\beta_r\rangle$  extracted in the framework of EV-SHGM

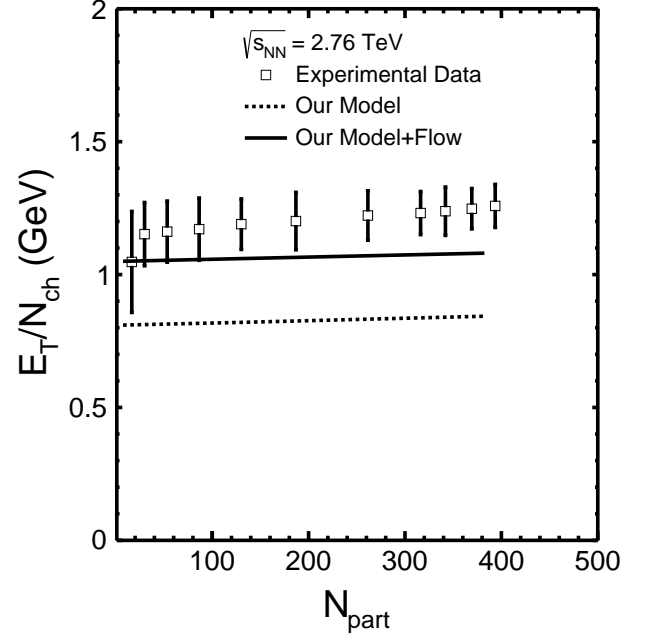


FIG. 9: Transverse energy per charged particle vs  $N_{part}$  for Pb-Pb collisions at  $\sqrt{s_{NN}} = 2.76$  TeV. Symbols are the experimental data [20]. The solid line is the result of our model calculations with flow and dotted line is that obtained in our model calculation without flow.

with respect to  $\sqrt{s_{NN}}$  from lower AGS energies to LHC energies. We notice that it increases monotonically with the collision energy with its lowest value at AGS to the highest value at LHC. This shows significant collectivity in high energy heavy-ion collisions. We fit a phenomenologically motivated power-law function, *i. e.*  $a + b(\sqrt{s_{NN}})^c$  to the energy dependence of  $\langle\beta_r\rangle$ . Here,  $a$ ,  $b$  and  $c$  are the fit parameters. For the best fit we get,  $a = 0.072 \pm 0.057$ ,  $b = 0.141 \pm 0.049$ , and  $c = 0.148 \pm 0.029$ . The predicted value of  $\langle\beta_r\rangle$  at  $\sqrt{s_{NN}} = 5.02$  TeV is 0.569 for the top central Pb+Pb collisions.

Figure 9 demonstrates the centrality dependence of  $E_T/N_{ch}$  for Pb-Pb collisions at  $\sqrt{s_{NN}}=2.76$  TeV. We calculate  $E_T/N_{ch}$  vs  $N_{part}$  using the same value of  $T$  and  $\mu_B$  as used in fitting the hadron ratios with respect to  $N_{part}$  at this energy. We compare EV-SHGM predictions with the experimental data [20] and find that it could not explain the data over all the number of participants. These findings suggest that we need to incorporate collective flow in EV-SHGM to explain the centrality dependence of  $E_T/N_{ch}$  at LHC energies. After comparison with data, we find that our model with flow explains the data very well over all the centrality bins within the experimental uncertainties. In ref. [39], it is argued that in a kinetic freeze-out scenario, the temperature should depend on centrality because during the kinetic freeze-out process there is a competition between local scattering and global expansion. Thus, the kinetic temperature is sensitive to the freeze-out process and hence centrality dependent.

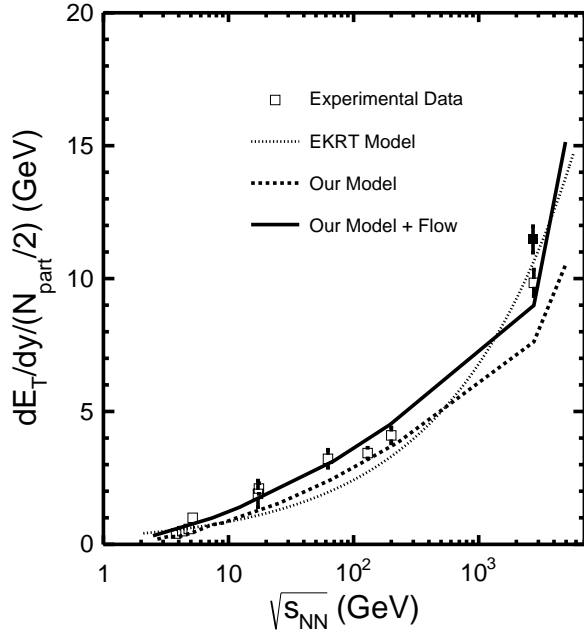


FIG. 10: The variation of  $dE_T/dy$  per number of participant with respect to  $\sqrt{s_{NN}}$  for the most central collisions. Solid line represents our model calculation with flow and dashed line is the result obtained in our model without flow. Dotted line presents the results of EKRT model. Symbols are the experimental data points [20].

In the case of chemical freeze-out, the temperature is observed to be centrality independent [40]. This is because during this process, the chemical reactions decrease abruptly leaving behind the chemically frozen state at the freeze-out and thus the chemical freeze-out temperature is insensitive to the collective dynamics but depends on thermodynamical variables. The observation of a centrality independence of  $E_T/N_{ch}$  at RHIC and LHC thus indicates to the chemical freeze-out scenario. This argument could be strengthened further in the subsequent section, when we make a direct comparison of  $E_T/N_{ch}$  values with the universal freeze-out criteria.

In figure 10, we present the variations of  $((dE_T/dy)/0.5N_{part})$  with respect to  $\sqrt{s_{NN}}$  over a broad energy range from AGS to LHC energies. We compare our model predictions with the experimental data [20]. The open symbol in the figure at  $\sqrt{s_{NN}} = 2.76$  TeV represents the ALICE data while solid symbol is the measurement by the CMS experiment. Here, we take care of conversion of the  $dE_T/d\eta$  to  $dE_T/dy$  by using the Jacobian factor  $J(\eta, y)$ , which is 1.09 at LHC [41]. We notice that our model results agree well with the data upto RHIC energies while it is unsuccessful in explaining the LHC data. Now, we show the results obtained after incorporating the collective flow in our model and find that it explains the ALICE data [20] within experimental error but lies below to CMS data [41] at LHC. We also show the results obtained in the

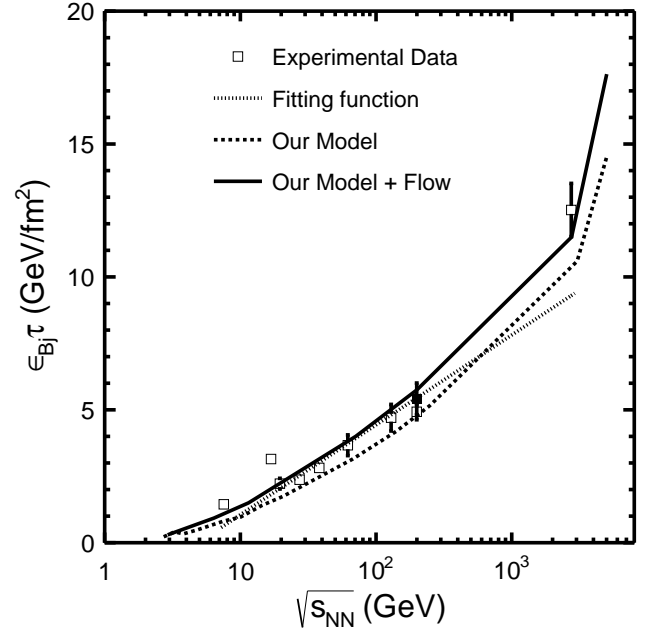


FIG. 11: The variation of  $\epsilon_{Bj}\tau$  with respect to  $\sqrt{s_{NN}}$  for the most central collisions. Solid line represents our model calculation with flow and dashed line is the result obtained in our stationary thermal model. The dotted line represents the result of the logarithmic fitting function as described in the text. Symbols are the experimental data points [10, 20, 21].

EKRT model [42] which is based on the calculation of perturbative QCD with gluon saturation mechanism and hydrodynamics. We observe that the EKRT model underestimates the experimental data upto top RHIC energy but seems to explain the data at LHC energies.

Figure 11 represents the variations of the product of Bjorken energy density ( $\epsilon_{Bj}$ ) and formation time ( $\tau$ ) with respect to  $\sqrt{s_{NN}}$  from AGS to LHC energies. Furthermore, our model explains the experimental data [10, 20, 21] very well upto RHIC energies while it fails to explain the data at LHC energies. We also show the results obtained after incorporating collective flow in our model and found a very good agreement with experimental data including that at LHC. We also fit the experimental data using the logarithmic function  $A + B \ln(\sqrt{s_{NN}})$ , where  $A = -2.32 \pm 0.51$  and  $B = 1.46 \pm 0.12$  are fit parameters. We notice that this function fits the data only upto RHIC energies and fails at LHC energies which suggests that logarithmic behaviour is not valid at LHC energies in this case. This could be an indication of a different particle production mechanism playing a role at LHC energies, which needs further investigations.

In figure 12, we demonstrate the ratio  $E_T/N_{ch}$  for the most central collisions with respect to  $\sqrt{s_{NN}}$  starting from lower AGS energies to LHC energies. We confront EV-SHGM calculations with the experimental data [10, 20, 21, 41]. Here, the solid symbol at LHC is the



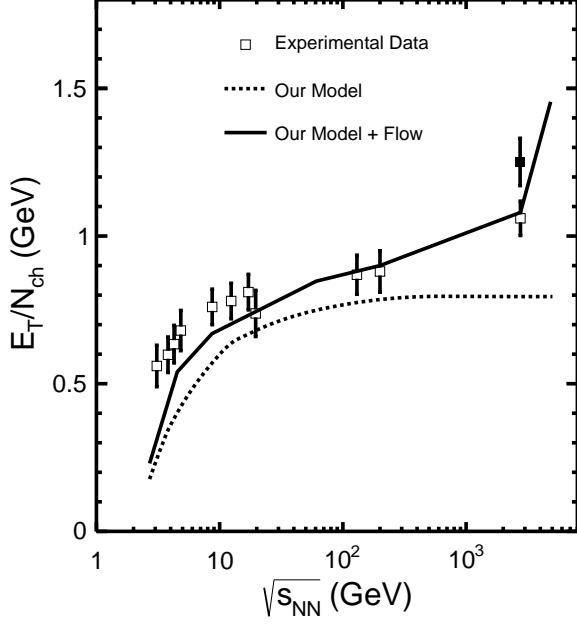


FIG. 12: Transverse energy per charged particle ( $E_T/N_{ch}$ ) as a function of collision energy  $\sqrt{s_{NN}}$ . Experimental data are compared with the expectations from EV-SHGM with and without the effect of collective flow.

CMS data while open symbol is the ALICE data. The model seems to explain the data at SPS and RHIC energies but fails at LHC energies. These findings may hint for possible non-equilibrium phenomena playing an important role at LHC. We also show the results obtained in our thermal model with the effect of flow. We notice that our model with flow explains the ALICE data [20] within the experimental errors while it could not explain the CMS data [41] at LHC energies, which indicates a more precise estimation of  $E_T/N_{ch}$  at the LHC.

We have studied the average transverse momentum ( $\langle p_T \rangle$ ) of hadrons in EV-SHGM with and without the effect of flow to understand the increase in  $E_T/N_{ch}$  from RHIC to LHC. Figure 13 demonstrates the  $N_{part}$  dependence of average transverse momentum ( $\langle p_T \rangle$ ) of charged hadrons at top RHIC and LHC  $\sqrt{s_{NN}} = 2.76$  TeV energies. The lines are model calculations and symbols are the experimental data [19, 43]. We find that, there is an almost 63% increase in  $\langle p_T \rangle$  from top RHIC to LHC at 2.76 TeV energy in EV-SHGM model with collective flow. We also get an almost 57% increase in  $\langle \beta_r \rangle$  from top RHIC to LHC at 2.76 TeV, which could be the reason for increase in  $\langle p_T \rangle$ . Further, no change in  $\langle p_T \rangle$  is observed in a static SHGM model from RHIC to LHC. This is because a static SHGM uses  $T$  and  $\mu_B$  as the inputs for the estimation of various thermodynamical observables. From top RHIC to LHC energies  $T$  and  $\mu_B$  are found to be constant within systematics [44]. This reveals that the increase in  $E_T/N_{ch}$  at LHC could be explained by the increase in  $\langle p_T \rangle$  and the collective flow. Here, we take all

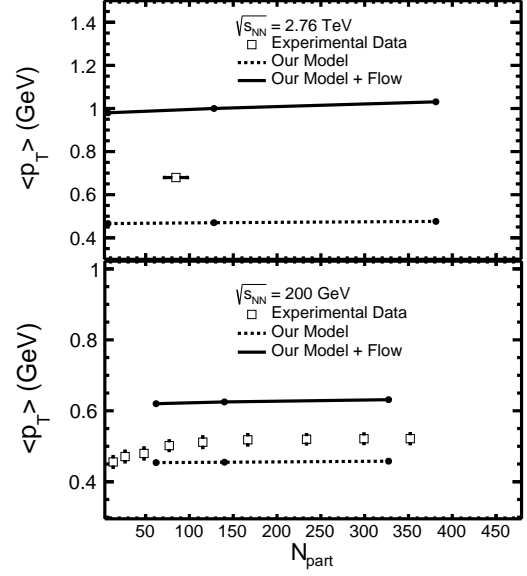


FIG. 13: Variations of average transverse momentum ( $\langle p_T \rangle$ ) with respect to  $N_{part}$  at  $\sqrt{s_{NN}} = 200$  GeV and 2.76 TeV. Symbols are the experimental data and lines are model results.

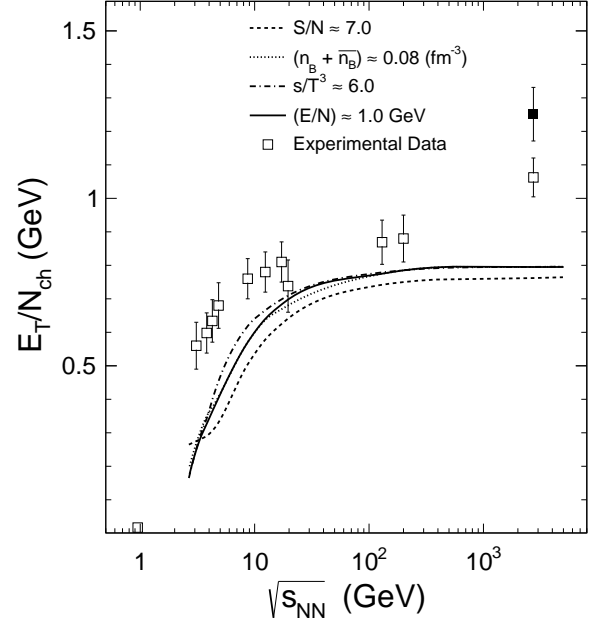


FIG. 14: The comparison between the experimental data on  $E_T/N_{ch}$  and the expectations from various universal freeze-out criteria in EV-SHGM.

the hadrons in our model while calculating the  $\langle p_T \rangle$  and take assumption of centrality independent  $\langle \beta_r \rangle$ .

#### IV. $E_T/N_{ch}$ AND FREEZE-OUT

In this section, we discuss the comparison of the experimental data on the ratio  $E_T/N_{ch}$  with that calculated in EV-SHGM using the various universal freeze-out criteria. Various observables such as the energy per hadrons  $(E/N) \approx 1.0$  [45, 46], the sum of baryons and antibaryons  $(n_B + n_{\bar{B}}) \approx 0.12/fm^3$  [47], the normalized entropy density,  $s/T^3 \approx 7.0$  [48], and the entropy per hadron  $(S/N) \approx 7.0$  [26] are proposed as universal freeze-out criteria in heavy-ion collisions. These observables are almost independent of  $\sqrt{s_{NN}}$  except at lower energies. In figure 14, we show the variations of  $E_T/N_{ch}$  with  $\sqrt{s_{NN}}$  from AGS to LHC energies. Here, the symbols are the experimental data while the lines are those calculated using various freeze-out criteria in our excluded-volume model. In our model, the values of these criteria are different than that mentioned above in the text, which are shown in the figure. We find a similar behaviour between the experimental data and those calculated using freeze-out criteria [49] in our model upto top RHIC energy, while at LHC energies our calculations could not explain the experimental data. This points to further investigation(s) to understand the possible reason(s) for the deviation of LHC data from the universal freeze-out criteria.

#### V. SUMMARY AND CONCLUSION

In summary, we have performed the calculation of global observables like transverse energy of hadrons, charged particle multiplicity and their ratios at midrapidity using our statistical-thermal model. We study the centrality dependence of various hadron ratios using our model and extract  $T$  and  $\mu_B$  at RHIC and LHC energies. We use the same value of  $T$  and  $\mu_B$  to study the centrality dependence of the ratio  $E_T/N_{ch}$  at those energies. Then we calculate the transverse mass spectra of  $\pi^-$  at various  $\sqrt{s_{NN}}$ , except at  $\sqrt{s_{NN}} = 2.7$  GeV where the transverse mass spectra of  $\pi^+$  is calculated by using EVSHGM. We get the average radial flow velocity at various energies by comparing our calculations with the experimental data. Once, we get the radial flow velocity

we study the transverse energy per unit rapidity. We also calculate the Bjorken energy density using our model at various  $\sqrt{s_{NN}}$ . Finally, we calculate the ratio  $E_T/N_{ch}$  at various energies using our excluded-volume SHGM with and without flow. Further we study various freeze-out criteria in the framework of EV-SHGM using  $E_T/N_{ch}$  as the observable.

In conclusion, we successfully describe the  $N_{part}$  dependence of various hadron ratios using our excluded-volume model. We observe that although the model describes the RHIC centrality data for the ratio,  $E_T/N_{ch}$ , it fails to explain the LHC data at  $\sqrt{s_{NN}} = 2.76$  TeV. The inclusion of the collective flow in our model, however qualitatively explains the centrality data at the LHC successfully, with some degree of deviations for higher centrality. While studying the energy dependence of  $E_T/N_{ch}$ , we observe that the excluded-volume hadron gas model with radial flow does not explain the CMS data at the LHC, whereas the ALICE data at the same energy is well-explained. This necessitates for precision measurement of  $E_T/N_{ch}$  at LHC energies to see if mechanisms other than the collective flow play a role. The energy dependence of Bjorken energy density, pseudorapidity densities of charged particles and transverse energy and total charged particle multiplicity showing deviations from a logarithmic behaviour [9, 50–56] at LHC may indicate different multiparticle production mechanism at LHC, compared to that at RHIC and lower collision energies. The observed increase in  $E_T/N_{ch}$  from RHIC to LHC is attributed due to an increase in  $\langle p_T \rangle$  and the onset of higher collective flow at the LHC. Our comparison of energy dependence of  $E_T/N_{ch}$  with various universal freeze-out criteria reveals that further investigations are necessary in order to have a proper understanding of the LHC data and its connection with freeze-out.

#### VI. ACKNOWLEDGEMENT

The authors would like to acknowledge Dr. Aditya Nath Mishra and Dr. Deepika Jena for careful reading of the manuscript and providing useful comments.

- 
- [1] I. Arsene *et al.* [BRAHMS Collaboration], Nucl. Phys. A **757**, 1 (2005).
  - [2] B. B. Back *et al.*, Nucl. Phys. A **757**, 28 (2005).
  - [3] J. Adams *et al.* [STAR Collaboration], Nucl. Phys. A **757**, 102 (2005).
  - [4] K. Adcox *et al.* [PHENIX Collaboration], Nucl. Phys. A **757**, 184 (2005).
  - [5] G. Policastro, D. T. Son and A. O. Starinets, Phys. Rev. Lett. **87**, 081601 (2001).
  - [6] V. Khachatryan *et al.* [CMS Collaboration], Phys. Lett. B **765**, 193 (2017).
  - [7] B. Abelev *et al.* [ALICE Collaboration], Phys. Rev. Lett. **109**, 072301 (2012).
  - [8] J. Cleymans, R. Sahoo, D. P. Mahapatra, D. K. Srivastava and S. Wheaton, Phys. Lett. B **660**, 172 (2008).
  - [9] R. Sahoo, and A. N. Mishra, Int. J. Mod. Phys. E **23**, 1450024 (2014).
  - [10] R. Sahoo, A. N. Mishra, N. K. Behera and B. K. Nandi, Adv. High Energy Phys. **2015**, 612390 (2015).
  - [11] S. K. Tiwari and R. Sahoo, Eur. Phys. J. A **52**, no. 12, 365 (2016).
  - [12] D. Prorok, Eur. Phys. J. A **24**, 93 (2005).
  - [13] D. Prorok, Eur. Phys. J. A **26**, 277 (2005).
  - [14] D. Prorok, Phys. Rev. C **75**, 014903 (2007).

- [15] M. Mishra and C. P. Singh, Phys. Rev. C **78**, 024910 (2008).
- [16] S. K. Tiwari and C. P. Singh, Adv. High Energy Phys. **2013**, 805413 (2013).
- [17] S. K. Tiwari and C. P. Singh, J. Phys. Conf. Ser. **509**, 012097 (2014).
- [18] S. K. Tiwari, P. K. Srivastava and C. P. Singh, J. Phys. G **40**, 045102 (2013).
- [19] J. Adams *et al.* [STAR Collaboration], Phys. Rev. C **70**, 054907 (2004).
- [20] J. Adam *et al.* [ALICE Collaboration], Phys. Rev. C **94**, 034903 (2016).
- [21] S. S. Adler *et al.* [PHENIX Collaboration], Phys. Rev. C **71**, 034908 (2005) Erratum: [Phys. Rev. C **71**, 049901 (2005)].
- [22] E. Schnedermann, J. Sollfrank, and U. Heinz, Phys. Rev. C **48**, 2462 (1993).
- [23] P. Braun-Munzinger *et al.*, Phys. Lett. B **344**, 43 (1995).
- [24] K. Adcox *et al.*, (PHENIX Collaboration), Phys. Rev. C **69**, 024904 (2004).
- [25] D. Kharzeev and M. Nardi, Phys. Lett. B **507**, 121 (2001).
- [26] S. K. Tiwari, P. K. Srivastava and C. P. Singh, Phys. Rev. C **85**, 014908 (2012).
- [27] I. Arsene *et al.* [BRAHMS Collaboration], Phys. Rev. C **72**, 014908 (2005).
- [28] J. Cleymans, B. Kampfer, M. Kaneta, S. Wheaton and N. Xu, Phys. Rev. C **71**, 054901 (2005).
- [29] B. Abelev *et al.* [ALICE Collaboration], Phys. Rev. C **88**, 044910 (2013).
- [30] S. Chatterjee, S. Das, L. Kumar, D. Mishra, B. Mohanty, R. Sahoo and N. Sharma, Adv. High Energy Phys. **2015**, 349013 (2015) and references therein.
- [31] G. L. Ma and Z. W. Lin, Phys. Rev. C **93**, 054911 (2016).
- [32] D. Adamova *et al.*, (CERES Collaboration), Phys. Rev. Lett. **90**, 022301 (2003).
- [33] P. Braun-Munzinger, A. Kalweit, K. Redlich and J. Stachel, Phys. Lett. B **747**, 292 (2015).
- [34] Y. B. Ivanov, Phys. Rev. C **89**, no. 2, 024903 (2014).
- [35] L. Kumar [STAR Collaboration], Nucl. Phys. A **931**, 1114 (2014).
- [36] B. I. Abelev *et al.* [STAR Collaboration], Phys. Rev. C **79**, 034909 (2009).
- [37] S. V. Afanasiev *et al.* [NA49 Collaboration], Phys. Rev. C **66**, 054902 (2002).
- [38] C. Alt *et al.* [NA49 Collaboration], Phys. Rev. C **73**, 044910 (2006).
- [39] U. W. Heinz and G. Kestin, Eur. Phys. J. ST **155**, 75 (2008).
- [40] J. Adams *et al.* [STAR Collaboration], Phys. Rev. Lett. **92**, 112301 (2004).
- [41] S. Chatrchyan *et al.* [CMS Collaboration], Phys. Rev. Lett. **109**, 152303 (2012).
- [42] K. J. Eskola, K. Kajantie, P. V. Ruuskanen and K. Tuominen, Nucl. Phys. B **570**, 379 (2000).
- [43] B. B. Abelev *et al.* [ALICE Collaboration], Phys. Lett. B **727**, 371 (2013).
- [44] B. Abelev *et al.* [ALICE Collaboration], Phys. Rev. Lett. **109**, 252301 (2012).
- [45] J. Cleymans and K. Redlich, Phys. Rev. Lett. **81**, 5284 (1998).
- [46] J. Cleymans, H. Oeschler, K. Redlich and S. Wheaton, Phys. Rev. C **73**, 034905 (2006).
- [47] P. Braun-Munzinger and J. Stachel, J. Phys. G **28**, 1971 (2002).
- [48] A. Tawfik, J. Phys. G **31**, S1105 (2005).
- [49] J. Cleymans, R. Sahoo, D. P. Mahapatra, D. K. Srivastava and S. Wheaton, J. Phys. G **35**, 104147 (2008).
- [50] A. N. Mishra, R. Sahoo, E. K. G. Sarkisyan and A. S. Sakharov, Eur. Phys. J. C **74**, 3147 (2014) Erratum: [Eur. Phys. J. C **75**, 70 (2015)].
- [51] E. K. G. Sarkisyan, A. N. Mishra, R. Sahoo and A. S. Sakharov, Phys. Rev. D **94**, 011501 (2016).
- [52] E. K. G. Sarkisyan, A. N. Mishra, R. Sahoo and A. S. Sakharov, Phys. Rev. D **93**, 054046 (2016); Addendum: [Phys. Rev. D **93**, no. 7, 079904 (2016)].
- [53] E. Abbas *et al.* [ALICE Collaboration], Phys. Lett. B **726**, 610 (2013).
- [54] S. Chatrchyan *et al.* [CMS Collaboration], JHEP **1108**, 141 (2011).
- [55] G. Aad *et al.* [ATLAS Collaboration], Phys. Lett. B **710**, 363 (2012).
- [56] K. Aamodt *et al.* [ALICE Collaboration], Phys. Rev. Lett. **105**, 252301 (2010).